

# A gentle introduction to the functional renormalization group: the Kondo effect in quantum dots

Sabine Andergassen, Tilman Enss, Christoph Karrasch and Volker Meden

**Abstract** The functional renormalization group provides an efficient description of the interplay and competition of correlations on different energy scales in interacting Fermi systems. An exact hierarchy of flow equations yields the gradual evolution from a microscopic model Hamiltonian to the effective action as a function of a continuously decreasing energy cutoff. Practical implementations rely on suitable truncations of the hierarchy, which capture nonuniversal properties at higher energy scales in addition to the universal low-energy asymptotics. As a specific example we study transport properties through a single-level quantum dot coupled to Fermi liquid leads. In particular, we focus on the temperature  $T = 0$  gate voltage dependence of the linear conductance. A comparison with exact results shows that the functional renormalization group approach captures the broad resonance plateau as well as the emergence of the Kondo scale. It can be easily extended to more complex setups of quantum dots.

## 1 Introduction

The coupling of a quantum dot with spin degenerate levels and local Coulomb interaction (modeled, e.g., by the single-impurity Anderson model; SIAM) to metallic

---

Sabine Andergassen  
Max-Planck-Institut für Festkörperforschung, D-70569 Stuttgart, Germany, and  
Laboratoire d'Etudes des Propriétés Electroniques des Solides, CNRS, BP 166, 38042 Grenoble,  
France

Tilman Enss  
INFN-SMC-CNR and Dipt. di Fisica, Università di Roma "La Sapienza", P.le Aldo Moro 5,  
I-00185 Roma, Italy

Christoph Karrasch and Volker Meden  
Institut für Theoretische Physik, Universität Göttingen, Friedrich-Hund-Platz 1,  
D-37077 Göttingen, Germany

leads gives rise to Kondo physics [1]. At low temperatures and for sufficiently high barriers the local Coulomb repulsion  $U$  leads to a broad resonance plateau in the linear conductance  $G$  of such a setup as a function of a gate voltage  $V_g$  which linearly shifts the level positions [2, 3, 4, 5, 6]. It replaces the Lorentzian found for noninteracting electrons. On resonance the dot is half-filled implying a local spin- $\frac{1}{2}$  degree of freedom responsible for the Kondo effect [1]. For the SIAM the zero temperature conductance is proportional to the one-particle spectral weight of the dot at the chemical potential [7]. The appearance of the plateau in the conductance is due to the pinning of the Kondo resonance in the spectral function at the chemical potential for  $-U/2 \lesssim V_g \lesssim U/2$  (here  $V_g = 0$  corresponds to the half-filled dot case) [1, 6]. Kondo physics in transport through quantum dots was confirmed experimentally [8, 9], and theoretically using the Bethe ansatz [2, 6] and the numerical renormalization-group (NRG) technique [10, 11]. However, both methods can hardly be used to study more complex setups. In particular, the extension of the NRG to more complex geometries beyond single-level quantum-dot systems [5, 6, 12] is restricted by the computational complexity which increases sharply with the number of interacting degrees of freedom. Alternative methods which allow for a systematic investigation are therefore required. We here propose the functional renormalization group (fRG) approach to study low-temperature transport properties through mesoscopic systems with local Coulomb correlations.

A particular challenge in the description of quantum dots is their distinct behavior on different energy scales, and the appearance of collective phenomena at new energy scales not manifest in the underlying microscopic model. An example of this is the Kondo effect where the interplay of the localized electron spin on the dot and the spin of the lead electrons leads to an exponentially (in  $U$ ) small scale  $T_K$ . This diversity of scales cannot be captured by straightforward perturbation theory. One tool to cope with such systems is the renormalization group: by treating different energy scales successively, one can often find an efficient description for each one. We will here give an introduction to one particular variant, the fermionic fRG [13], which is formulated in terms of an exact hierarchy of coupled flow equations for the vertex functions as the energy scale is lowered. The flow starts directly from the microscopic model, thus including nonuniversal effects on higher energy scales from the outset, in contrast to effective field theories capturing only the asymptotic behavior. As the cutoff scale is lowered, fluctuations at lower energy scales are successively included until one finally arrives at the full effective action (the generating functional of the one-particle irreducible vertex functions) from which all physical properties can be extracted. This allows to control infrared singularities and competing instabilities in an unbiased way. Truncations of the flow equation hierarchy and suitable parametrizations of the frequency and momentum dependence of the vertex functions lead to powerful new approximation schemes, which are justified for weak renormalized interactions. A comparison with exact results shows that the fRG is remarkably accurate even for sizeable interactions.

The outline of this article is as follows. In Sec. 2 we introduce the fRG formalism and derive the hierarchy of flow equations. The implementation of the fRG technique for a quantum dot modeled by a SIAM is described in Sec. 3. In the following

we present results for the linear conductance including a comparison with exact solutions and discuss the emergence of the Kondo scale. We conclude in Sec. 4 with a summary and outlook on further applications and extensions of the present work.

## 2 The fRG technique

To make this article self-contained, this section aims to give a very short introduction into the fRG *formalism* by deriving the functional flow equations. Readers not so much interested in the formal beauty might jump ahead to the following Sec. 3 where these flow equations are applied to a specific physical model. An introduction to the many-body formalism used here can be found, e.g., in [14]; for the details of the derivation of the functional flow equation see, e.g., [15, 16] and references therein. Exact functional flow equations were derived for bosonic field theories in [17, 18, 19] and for fermionic fields in the one-particle irreducible scheme in [13].

### 2.1 Green and vertex functions

We consider a system of interacting fermions described by Grassmann variables  $\psi$ ,  $\bar{\psi}$ , and an action

$$S[\psi, \bar{\psi}] = (\bar{\psi}, C^{-1}\psi) - V[\psi, \bar{\psi}] \quad (1)$$

with bare propagator

$$C(K) = \frac{1}{i\varepsilon - \xi_{\mathbf{k}}} \quad (2)$$

where the index  $K = (\varepsilon, \mathbf{k}, \sigma)$  collects the Matsubara frequency  $\varepsilon$  and the quantum numbers of a suitable single-particle basis set, e.g., momentum  $\mathbf{k}$  and spin projection  $\sigma$ , and  $\xi_{\mathbf{k}} = \varepsilon_{\mathbf{k}} - \mu$  denotes the energy relative to the chemical potential. In order to understand the general structure of the flow equation it is useful to include a Nambu (particle/hole) index into  $K$ : then each directed fermion line denotes the propagation of either a particle or a hole [13]. The inner product implies a summation over these indices: for our diagonal propagator,  $(\bar{\psi}, C^{-1}\psi) = \sum_K \bar{\psi}_K C_K^{-1} \psi_K$ .  $V[\psi, \bar{\psi}]$  is an arbitrary many-body interaction; we will see a specific example for this below in Eq. (17). Connected Green functions can be obtained from the generating functional [14]

$$\mathcal{G}[\eta, \bar{\eta}] = -\log \left\{ \mathcal{N} \int D\bar{\psi}\psi e^{S[\psi, \bar{\psi}]} e^{-(\bar{\psi}, \eta) - (\bar{\eta}, \psi)} \right\} \quad (3)$$

by taking derivatives with respect to the source fields  $\eta$ :

$$\begin{aligned}
G_m(K'_1, \dots, K'_m; K_1, \dots, K_m) &= -\langle \Psi_{K'_1} \dots \Psi_{K'_m} \bar{\Psi}_{K_m} \dots \bar{\Psi}_{K_1} \rangle_{\text{conn}} \\
&= \frac{\delta^m}{\delta \eta_{K_1} \dots \delta \eta_{K_m}} \frac{\delta^m}{\delta \bar{\eta}_{K'_1} \dots \delta \bar{\eta}_{K'_m}} \mathcal{G}[\eta, \bar{\eta}] \Big|_{\eta=\bar{\eta}=0}.
\end{aligned}$$

Equivalently,  $\mathcal{G}[\eta, \bar{\eta}]$  can be expanded in powers of the source fields with expansion coefficients  $G_m(K'_1, \dots, K_m)$ . The normalization factor  $\mathcal{N} = \det C$  cancels the noninteracting vacuum diagrams, such that  $\mathcal{G}[0, 0] = 0$  in the absence of interaction. As we explain below, it will be of advantage in our case to describe the system not by connected Green functions but by the one-particle irreducible (1PI) vertex functions. Their generating functional, the *effective action*, is obtained from  $\mathcal{G}$  by Legendre transformation,

$$\Gamma[\phi, \bar{\phi}] = \mathcal{G}[\eta, \bar{\eta}] + (\bar{\phi}, \eta) - (\bar{\eta}, \phi). \quad (4)$$

This functional can again be expanded in powers of the fields  $\phi, \bar{\phi}$  to obtain the vertex functions  $\gamma_m(K'_1, \dots, K_m)$ . The usual relations between  $\mathcal{G}$  and  $\Gamma$  hold, i.e.,  $\phi = \delta \mathcal{G} / \delta \bar{\eta}$ ,  $\bar{\phi} = \delta \mathcal{G} / \delta \eta$  as well as  $\bar{\eta} = \delta \Gamma / \delta \phi$ ,  $\eta = \delta \Gamma / \delta \bar{\phi}$ , and  $\delta^2 \Gamma / \delta \phi \delta \bar{\phi} = (\delta^2 \mathcal{G} / \delta \eta \delta \bar{\eta})^{-1}$ .

## 2.2 Functional flow equations

We introduce an infrared cutoff into the bare propagator that suppresses all soft modes, which may be a source of divergences in perturbation theory. In bulk systems it is convenient to use a momentum cutoff, which suppresses momenta close to the Fermi surface. On the other hand, if translation invariance is spoiled by impurities or a particular spatial setup as for quantum dots, it is easier to use a frequency cutoff, excluding all Matsubara frequencies below scale  $\Lambda$  using a step function  $\Theta(x)$ :

$$C^\Lambda(K) = \frac{\Theta(|\varepsilon| - \Lambda)}{i\varepsilon - \xi_k}. \quad (5)$$

This changes the microscopic model to exclude soft modes; in the limit  $\Lambda \rightarrow 0$  the original model is recovered. The easiest way to understand how the Green functions change with  $\Lambda$  is to derive the flow equation for the cutoff-dependent generating functional

$$\mathcal{G}^\Lambda[\eta, \bar{\eta}] = -\log \left\{ \mathcal{N}^\Lambda \int D\bar{\psi} \psi e^{(\bar{\psi}, Q^\Lambda \psi) - V[\psi, \bar{\psi}]} e^{-(\bar{\psi}, \eta) - (\bar{\eta}, \psi)} \right\} \quad (6)$$

with  $(C^\Lambda)^{-1} \equiv Q^\Lambda$ , and the normalization factor  $\mathcal{N}^\Lambda = (\det Q^\Lambda)^{-1}$ . Taking the  $\Lambda$  derivative and denoting  $\partial_\Lambda Q^\Lambda = \dot{Q}^\Lambda$ ,

$$\begin{aligned}
\partial_\Lambda \mathcal{G}^\Lambda &= -\partial_\Lambda \log \mathcal{N}^\Lambda - \frac{1}{e^{-\mathcal{G}^\Lambda}} \int D\bar{\psi}\psi \left( \bar{\psi}, \dot{Q}^\Lambda \psi \right) e^{(\bar{\psi}, \dot{Q}^\Lambda \psi) - V[\psi, \bar{\psi}] - (\bar{\psi}, \eta) - (\bar{\eta}, \psi)} \\
&= -\partial_\Lambda \log \mathcal{N}^\Lambda + e^{\mathcal{G}^\Lambda} \left( \frac{\delta}{\delta \eta}, \dot{Q}^\Lambda \frac{\delta}{\delta \bar{\eta}} \right) e^{-\mathcal{G}^\Lambda} \\
&= \text{Tr}(\dot{Q}^\Lambda C^\Lambda) - \text{Tr} \left( \dot{Q}^\Lambda \frac{\delta^2 \mathcal{G}^\Lambda}{\delta \eta \delta \bar{\eta}} \right) + \left( \frac{\delta \mathcal{G}^\Lambda}{\delta \eta}, \dot{Q}^\Lambda \frac{\delta \mathcal{G}^\Lambda}{\delta \bar{\eta}} \right)
\end{aligned} \tag{7}$$

where the first term,  $-\partial_\Lambda \log \mathcal{N}^\Lambda = \text{Tr}(\dot{Q}^\Lambda C^\Lambda)$ , comes from the derivative of the normalization factor, and the trace denotes a sum over all  $K$ .

In the present application to quantum dots, the one-particle potential is strongly renormalized, and it is important to include the feedback of this renormalization nonperturbatively in the flow equations. This is most easily achieved in the one-particle irreducible (1PI) scheme, where the one-particle renormalizations are included in the internal propagators. Hence, we perform a Legendre transform which now also depends on  $\Lambda$ ,

$$\Gamma^\Lambda[\phi, \bar{\phi}] = \mathcal{G}^\Lambda[\eta^\Lambda, \bar{\eta}^\Lambda] + \left( \bar{\phi}, \eta^\Lambda \right) - \left( \bar{\eta}^\Lambda, \phi \right), \tag{8}$$

and we find  $\partial_\Lambda \Gamma^\Lambda = d\mathcal{G}^\Lambda/d\Lambda + (\bar{\phi}, \partial_\Lambda \eta^\Lambda) - (\partial_\Lambda \bar{\eta}^\Lambda, \phi) = \partial_\Lambda \mathcal{G}^\Lambda$  after taking into account the derivatives also of the  $\eta^\Lambda$  fields. The fundamental variables of  $\Gamma^\Lambda$  are the  $\phi$  fields and the  $\eta$  acquire a  $\Lambda$  dependence via the relation between  $\phi$  and  $\eta$  [14]. By Legendre transform of the flow Eq. (7), we obtain the 1PI flow equation

$$\partial_\Lambda \Gamma^\Lambda[\phi, \bar{\phi}] = \partial_\Lambda \mathcal{G}^\Lambda = \text{Tr} \dot{Q}^\Lambda \left[ C^\Lambda - \left( \frac{\delta^2 \Gamma^\Lambda[\phi, \bar{\phi}]}{\delta \phi \delta \bar{\phi}} \right)^{-1} \right] + \left( \bar{\phi}, \dot{Q}^\Lambda \phi \right). \tag{9}$$

The inversion of a functional of Grassmann variables with a nonzero complex part is well defined as a geometric series, which involves only products of Grassmann variables. Therefore, we write the Hessian of  $\Gamma^\Lambda$  as

$$\frac{\partial^2 \Gamma^\Lambda}{\partial \phi_K \partial \bar{\phi}_{K'}} = (G^\Lambda)_{K, K'}^{-1} + \tilde{\Gamma}_{K, K'}^\Lambda[\phi, \bar{\phi}], \tag{10}$$

where the inverse full propagator  $(G^\Lambda)^{-1} = \gamma_1^\Lambda = Q^\Lambda - \Sigma^\Lambda$  according to the Dyson equation, and  $\tilde{\Gamma}^\Lambda$  depends at least quadratically on the  $\phi, \bar{\phi}$  fields. This decomposition allows us to write the inverse as a geometric series,

$$\left( \frac{\partial^2 \Gamma^\Lambda}{\partial \phi_K \partial \bar{\phi}_{K'}} \right)^{-1} = (1 + G^\Lambda \tilde{\Gamma}^\Lambda)^{-1} G^\Lambda = \left( 1 - G^\Lambda \tilde{\Gamma}^\Lambda + [G^\Lambda \tilde{\Gamma}^\Lambda]^2 - \dots \right) G^\Lambda,$$

which we insert into the flow Eq. (9),

$$\partial_\Lambda \Gamma^\Lambda = \text{Tr}(\dot{Q}^\Lambda [C^\Lambda - G^\Lambda]) + \left( \bar{\phi}, \dot{Q}^\Lambda \phi \right) + \text{Tr}(S^\Lambda [\tilde{\Gamma}^\Lambda - \tilde{\Gamma}^\Lambda G^\Lambda \tilde{\Gamma}^\Lambda + \dots]). \tag{11}$$

The first term describes the flow of the zero-point function (grand canonical potential), while the second term expresses the change of the bare propagator with  $\Lambda$ . The hierarchy of flow equations is encoded in the third term which represents a loop with an arbitrary number of vertices  $\tilde{\Gamma}^\Lambda$ , which contribute at least two external legs each, connected by full propagators  $G^\Lambda$  and one single-scale propagator  $S^\Lambda$  which has support only at frequency  $\Lambda$ ,

$$S^\Lambda = G^\Lambda \dot{Q}^\Lambda G^\Lambda. \quad (12)$$

Given the initial conditions at  $\Lambda = \infty$ , the flow equations determine  $\Gamma^\Lambda$  uniquely for all  $\Lambda < \infty$ . The flow of  $\Gamma^\Lambda$  thus interpolates between the bare action  $\Gamma^{\Lambda=\infty} = S$  and the full solution of the problem,  $\Gamma^{\Lambda=0} = \Gamma$ .

### 2.3 Flow equation hierarchy

Expanding the functional flow equation for  $\Gamma^\Lambda$  in powers of the source fields  $\phi, \bar{\phi}$ , we obtain an infinite hierarchy of coupled flow equations for the  $m$ -particle vertex functions  $\gamma_m^\Lambda$ . This hierarchy can be represented diagrammatically and the first three levels are shown in Fig. 1, where each line represents the propagation of either a particle or a hole. For instance, the last diagram in the second line includes both a particle-hole and a particle-particle bubble. For our application to the SIAM it is convenient to distinguish these<sup>1</sup>, so we denote by  $\gamma_2(1', 2'; 1, 2)$  the two-particle vertex with incoming electrons 1, 2 and outgoing electrons 1', 2'.

The first line of Fig. 1 represents the flow equation for the self-energy  $\Sigma^\Lambda$ ,

$$\frac{\partial}{\partial \Lambda} \Sigma^\Lambda(1', 1) = -T \sum_{2, 2'} e^{i\epsilon_2 0^+} S^\Lambda(2, 2') \gamma_2^\Lambda(1', 2'; 1, 2), \quad (13)$$

where the labels 1, 1', ... are a shorthand notation for  $K_1, K_{1'}$  etc., and the summation includes Matsubara frequencies. The two-particle vertex  $\gamma_2^\Lambda$  entering Eq. (13) is determined by the second line in Fig. 1, which in turn depends on the three-particle vertex  $\gamma_3^\Lambda$ , etc. This infinite system of coupled differential equations can usually not be integrated analytically; therefore one has to resort to numerical computations which require to truncate the hierarchy by neglecting the flow of the higher vertices. This may be justified perturbatively for weak interactions since the higher vertices not present in the bare interaction are generated only at higher orders in the effective interaction. As a first step, we consider only the flow of the self-energy with all higher vertices remaining at their initial conditions (the bare interaction  $V$ ): in our application, this already produces qualitatively the correct result. As a second step, we also include the flow of  $\gamma_2^\Lambda$  but neglect  $\gamma_3^\Lambda$ , which brings us even quantitatively within a few percent of the known results:

---

<sup>1</sup> A derivation of the flow equation using separate particle and hole propagators from the outset can be found, e.g., in [20].

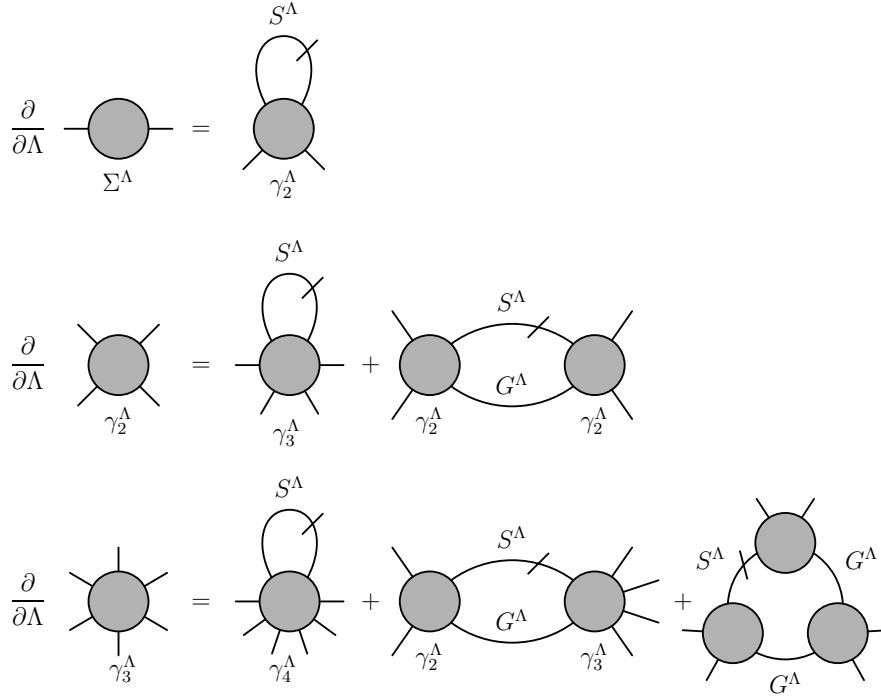


**Fig. 1** Diagrammatic representation of the flow equations for the self-energy  $\Sigma^\Lambda$ , the two-particle vertex  $\gamma_2^\Lambda$  and the three-particle vertex  $\gamma_3^\Lambda$  in the 1PI formulation of the fRG.

$$\begin{aligned} \frac{\partial}{\partial \Lambda} \gamma_2^\Lambda(1', 2'; 1, 2) = T \sum_{3,3'} \sum_{4,4'} G_{3,3'}^\Lambda S_{4,4'}^\Lambda & \left[ \gamma_2^\Lambda(1', 2'; 3, 4) \gamma_2^\Lambda(3', 4'; 1, 2) \right. \\ & \left. - \gamma_2^\Lambda(1', 4'; 1, 3) \gamma_2^\Lambda(3', 2'; 4, 2) + \gamma_2^\Lambda(2', 4'; 1, 3) \gamma_2^\Lambda(3', 1'; 4, 2) + (3 \leftrightarrow 4, 3' \leftrightarrow 4') \right], \end{aligned} \quad (14)$$

with the first term representing the particle-particle channel and the other two the particle-hole channels, respectively. The last bracket means that the two terms in the second line have to be repeated with the changes of variables as indicated.

There is one technical detail which allows to simplify these equations significantly: the sharp frequency cutoff in Eq. (5) has the advantage that the frequency integrals on the right-hand side of Eqs. (13) and (14) can be performed analytically. The propagators contain both  $\Theta(|\varepsilon| - \Lambda)$  and  $\delta(|\varepsilon| - \Lambda) = -\partial_\Lambda \Theta(|\varepsilon| - \Lambda)$  functions, which at first look ambiguous because the step function has a jump exactly where the  $\delta$  function has support. However, if one smoothes the step slightly and makes a change of variables from  $\Lambda$  to  $t = \Theta(|\varepsilon| - \Lambda)$  and  $dt = -\delta(|\varepsilon| - \Lambda)d\Lambda$  in the vicinity of  $|\varepsilon| = \Lambda$ , the integration over the step becomes well-defined and is implemented by the substitution [21, 15]

$$\delta(x - \Lambda) f(\Theta(x - \Lambda)) \rightarrow \delta(x - \Lambda) \int_0^1 f(t) dt. \quad (15)$$

Using this substitution, the product of full and single-scale propagators around the loop is replaced by a delta function<sup>2</sup>  $\delta(|\varepsilon| - \Lambda)$  times smooth propagators of the form

$$\tilde{G}^\Lambda = [G_0^{-1} - \Sigma^\Lambda]^{-1}. \quad (16)$$

Note that the explicit  $\Lambda$  dependence remains only in the self-energy, such that the resulting propagator (and hence the flow equation) is smooth in both  $\Lambda$  and  $\varepsilon$  and can be easily integrated numerically.

### 3 Application to quantum dots

In order to give a pedagogical example how the functional flow equations can be used to solve an interesting physical problem, we choose as a toy model the SIAM [3, 4], which is used to study, e.g., transport through a quantum dot. After integrating out the noninteracting lead degrees of freedom (see below) this model has zero space dimensions, hence spin is the only quantum number, and the resulting flow equations are particularly simple and can even be integrated analytically if the flow of the two-particle vertex is neglected. Nevertheless, the physics is nontrivial, and the exponentially small scale (the Kondo scale) we obtain is seen neither in perturbation theory in  $U$  (which in the present example is free of infrared divergencies) nor in self-consistent Hartree-Fock calculations.

#### 3.1 The single-impurity Anderson model

Our model consists of a single site with local Coulomb repulsion  $U \geq 0$ , which is connected to two leads  $l = L, R$  via tunnel barriers  $t_{L,R}$  (see Fig. 2):

$$H = U(n_\uparrow - \frac{1}{2})(n_\downarrow - \frac{1}{2}) + \sum_\sigma \varepsilon_\sigma d_\sigma^\dagger d_\sigma - \sum_{\sigma,l} t_l (d_\sigma^\dagger c_{0,l} + \text{H.c.}), \quad (17)$$

where  $d_\sigma^\dagger$  is the creation operator for an electron with spin  $\sigma$  on the dot,  $n_\sigma = d_\sigma^\dagger d_\sigma$  is the spin- $\sigma$  number operator, and  $c_l^\dagger$  denotes the creation operator at the end of the semi-infinite lead  $l$ . The leads may be modeled by tight-binding chains,  $H_l = -t \sum_{m=0}^\infty (c_{m,l}^\dagger c_{m+1,l} + \text{h.c.})$  with hopping amplitude  $t$ . The hybridization of the dot with the leads broadens the levels on the dot by  $\Gamma_l(\varepsilon) = \pi t_l^2 \rho_l(\varepsilon)$ , where  $\rho_l(\varepsilon)$  is the local density of states at the end of lead  $l$  which we henceforth assume to be

---

<sup>2</sup> There remain additional frequency constraints if not all propagators are at the same frequency.

constant (wide-band limit). A local magnetic field  $h$  at the dot site splits the spin-up and spin-down energy levels around the gate voltage  $V_g$  ( $\sigma_{\uparrow\downarrow} = \pm 1$ ),

$$\varepsilon_{\uparrow\downarrow} = V_g + \sigma h/2. \quad (18)$$

Since the leads are noninteracting, we can integrate out the degrees of freedom of the lead electrons in the path integral and thereby obtain a hybridization contribution  $\Gamma = \Gamma_L + \Gamma_R$  to the bare Green function of the dot which depends only on the sign of the Matsubara frequency [1],

$$G_{0,\sigma}(i\varepsilon) = \frac{1}{i\varepsilon - (V_g + \sigma h/2) + i\Gamma \text{sgn}(\varepsilon)}. \quad (19)$$

By solving the interacting many-body problem we obtain a frequency-dependent self-energy  $\Sigma_\sigma(i\varepsilon)$  on the dot, and the full dot propagator is given by the Dyson equation,

$$G_\sigma(i\varepsilon) = [G_{0,\sigma}(i\varepsilon)^{-1} - \Sigma_\sigma(i\varepsilon)]^{-1}. \quad (20)$$

This self-energy could be computed by perturbation theory in the strength of the Coulomb interaction, e.g., in a Hartree-Fock calculation, but it turns out that this does not capture the physical effect that is observed in experiments and that we wish to describe. Instead, we will now show how the fRG can be used to compute with very little effort an approximation for the self-energy that leads to the correct physical properties of the  $T = 0$  conductance.

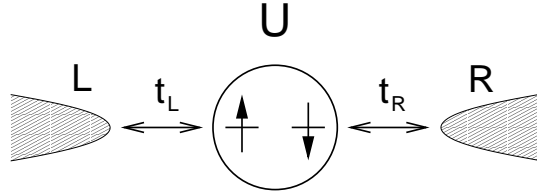


**Fig. 2** A quantum dot connected to two leads (reservoirs).

In general the linear response conductance is given by the current-current correlation function (Kubo formula). At zero temperature, zero bias voltage, and for a single interacting site the exact conductance has the simple form [7]

$$G(V_g) = G_\uparrow(V_g) + G_\downarrow(V_g) \quad (21)$$

$$G_\sigma(V_g) = \frac{e^2}{h} \pi \Gamma \rho_\sigma(0)$$

in terms of the dot spectral function continued analytically to real frequencies,

$$\rho_\sigma(\varepsilon) = -\frac{1}{\pi} \text{Im} G_\sigma(\varepsilon + i0^+). \quad (22)$$

### 3.2 Flow equation for the self-energy

In order to implement the fRG, following Eq. (5) we introduce a cutoff in Matsubara frequency into the bare propagator on the dot (19),

$$G_{0,\sigma}^{\Lambda}(i\varepsilon) = \frac{\Theta(|\varepsilon| - \Lambda)}{i\varepsilon - (V_g + \sigma h/2) + i\Gamma \operatorname{sgn}(\varepsilon)}. \quad (23)$$

This is an infrared cutoff which sets the propagator to zero for frequencies smaller than  $\Lambda$  (preventing these modes from being excited), but leaves the high-energy modes unchanged (propagating). As the cutoff scale  $\Lambda$  is gradually lowered, more and more low-energy degrees of freedom are included, until finally the original model is recovered for  $\Lambda \rightarrow 0$ . Changing the cutoff scale leads to the infinite hierarchy of flow equations for the vertex functions shown in Fig. 1. We use the flow equation for the self-energy (13) with the single-scale propagator substituted by (16). The two-particle vertex  $\gamma_2^{\Lambda}$  is in general a complicated function of three independent frequencies (justifying the name *functional* renormalization group) that evolves during the flow by the second line of Fig. 1. As a first approximation we neglect the flow of the two-particle vertex and all higher vertex functions. This can be justified perturbatively if the bare coupling  $U$  is small, as all the terms generated during the flow are of higher order in  $U$ . As a consequence, the two-particle vertex

$$\gamma_2^{\Lambda}(i\varepsilon\sigma, i\varepsilon'\bar{\sigma}; i\varepsilon\sigma, i\varepsilon'\bar{\sigma}) = U^{\Lambda} \quad (24)$$

remains for all  $\Lambda$  at its initial condition,  $U^{\Lambda} \equiv U^{\Lambda=\infty} = U$  which is the bare Coulomb interaction in the Hamiltonian (17). We denote  $\bar{\sigma} = -\sigma$ . As  $\gamma_2^{\Lambda}$  does not depend on frequency in our approximation, also the self-energy does not acquire a frequency dependence during the flow. The flow equation for the effective level position  $V_{\sigma}^{\Lambda} = V_g + \sigma h/2 + \Sigma_{\sigma}^{\Lambda}$  is

$$\begin{aligned} \partial_{\Lambda} V_{\sigma}^{\Lambda} &= -\frac{U^{\Lambda}}{2\pi} \int d\varepsilon \delta(|\varepsilon| - \Lambda) \tilde{G}_{\bar{\sigma}}^{\Lambda}(i\varepsilon) = -\frac{U^{\Lambda}}{2\pi} \sum_{\varepsilon=\pm\Lambda} \frac{1}{i\varepsilon - V_{\bar{\sigma}}^{\Lambda} + i\Gamma \operatorname{sgn}\varepsilon} \\ &= \frac{U^{\Lambda} V_{\bar{\sigma}}^{\Lambda} / \pi}{(\Lambda + \Gamma)^2 + (V_{\bar{\sigma}}^{\Lambda})^2} \end{aligned} \quad (25)$$

with initial condition  $V_{\sigma}^{\Lambda=\infty} = V_g + \sigma h/2$  [22]. At the end of the flow, the renormalized potential  $V_{\sigma} = V_{\sigma}^{\Lambda=0}$  determines the dot spectral function (22),

$$\rho_{\sigma}(\varepsilon) = \frac{1}{\pi} \frac{\Gamma}{(\varepsilon - V_{\sigma})^2 + \Gamma^2}, \quad (26)$$

which is a Lorentzian of full width  $2\Gamma$  and height  $1/\pi\Gamma$  centered around  $V_{\sigma}$ . Although the true spectral function has a very different form with a very sharp Kondo peak at  $\varepsilon = V_{\sigma}$ , this difference is not seen in the  $T = 0$  conductance (21): it probes only the value of the spectral function at the chemical potential  $\varepsilon = 0$ ,

$$G_{\sigma}(V_g) = \frac{e^2}{h} \frac{\Gamma^2}{V_g^2 + \Gamma^2}. \quad (27)$$

In the noninteracting case,  $V_{\sigma} = V_g + \sigma h/2$  and the conductance is a sum of two Lorentzians of the applied gate voltage. If interaction is switched on, this changes drastically.

In Fig. 3 the conductance  $G$  as a function of gate voltage  $V_g$  for the SIAM is shown for different values of  $U/\Gamma$  in the upper panel, together with the occupation of the dot in the lower, both for the case without magnetic field, implying  $V_{\uparrow}^{\Lambda} = V_{\downarrow}^{\Lambda} = V^{\Lambda}$  and  $G_{\uparrow} = G_{\downarrow}$ . For  $\Gamma \ll U$  the resonance exhibits a plateau [6]. In this region the occupation is close to 1 while it sharply rises/drops to 2/0 to the left/right of the plateau. Also for asymmetric barriers we reproduce the exact resonance height  $4\Gamma_L\Gamma_R/(\Gamma_L + \Gamma_R)^2 (2e^2/h)$  [1, 6]. Here we focus on strong couplings  $U/\Gamma \gg 1$ .

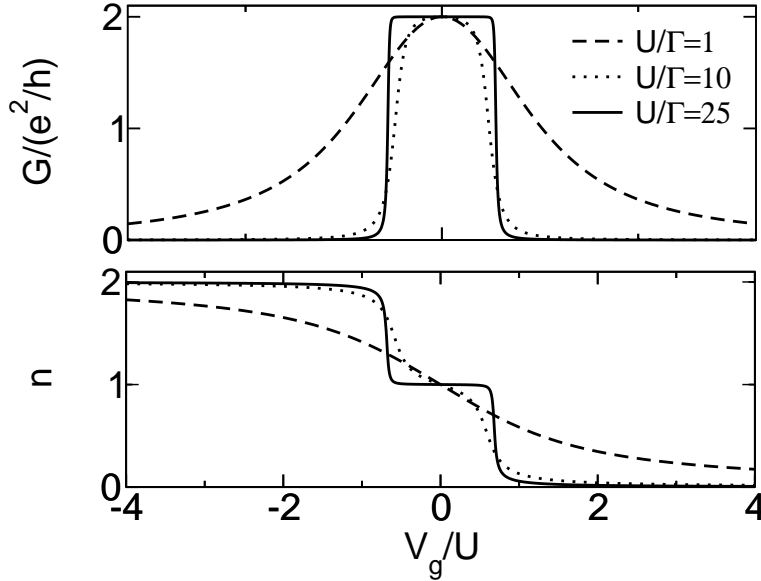


**Fig. 3** *Upper panel:* conductance as a function of gate voltage for different values of  $U/\Gamma$  and  $h = 0$ . *Lower panel:* average number of electrons on the dot.

The solution of the differential Eq. (25) at  $\Lambda = 0$  is obtained in implicit form

$$\frac{vJ_1(v) - \gamma J_0(v)}{vY_1(v) - \gamma Y_0(v)} = \frac{J_0(v_g)}{Y_0(v_g)}, \quad (28)$$

with  $v = V\pi/U$ ,  $v_g = V_g\pi/U$ ,  $\gamma = \Gamma\pi/U$ , and Bessel functions  $J_n, Y_n$ . For  $|V_g| < V_c$  this equation has a solution with small  $|V|$ , where  $v_c = V_c\pi/U$  is the first zero of  $J_0$  corresponding to  $V_c \simeq 0.77U$ . For  $U \gg \Gamma$  the crossover to a solution with  $|V|$  being of order  $U$  (for  $|V_g| > V_c$ ) is fairly sharp. Expanding both sides of Eq. (28) for small

$|v|$  and  $|v_g|$  gives

$$V = V_g \exp\left(-\frac{U}{\pi\Gamma}\right). \quad (29)$$

The consequent exponential pinning of the spectral weight in Eq. (22) at the chemical potential for small  $|V_g|$  and the sharp crossover to a  $V$  of order  $U$  when  $|V_g| > V_c$  leads to the observed resonance line shape represented by the dashed line in Fig. 4. For  $U \gg \Gamma$  the width of the plateau is  $2V_c \simeq 1.5U$ , which is larger than the width  $U$  found with the Bethe ansatz [2, 6] corresponding to the solid line in Fig. 4. Our approximation furthermore slightly overestimates the sharpness of the box-shaped resonance. The inclusion of the renormalization of the two-particle vertex improves the quantitative accuracy of the results considerably (see below), while the pinning of the spectral function and the subsequent resonance plateau is captured already at the first order of the flow-equation hierarchy, even though the spectral function neither shows the narrow Kondo resonance nor the Hubbard bands.

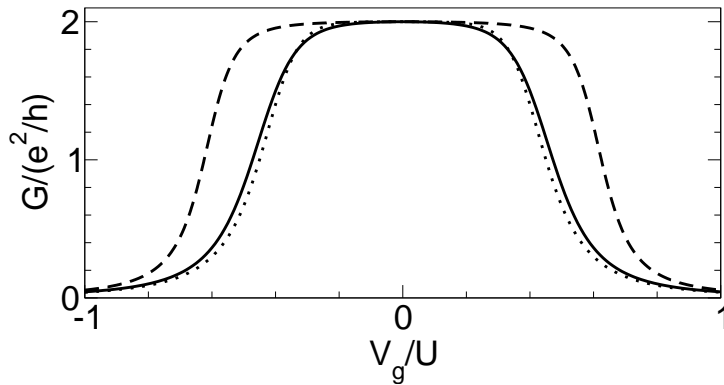


**Fig. 4** Gate voltage dependence of the conductance at  $U/\Gamma = 4\pi$  and  $h = 0$ . *Solid line*: exact Bethe ansatz solution from [6]. *Dashed line*: fRG approximation without flow of the interaction. *Dotted line*: fRG approximation with flow of vertex.

### 3.3 Flow equation for the fermion interaction

With the simple approximation above, we have obtained an exponentially small scale for the local potential from a renormalization group flow equation. This yields a plateau in the conductance that qualitatively agrees already well with the exact Bethe ansatz solution. We will now demonstrate how one can go beyond the simplest approximations in the renormalization group flow equations to improve (systematically for small  $U$ ) the result and the agreement with the known solutions. Any improvement of the flow equation has to come from a more detailed parametriza-

tion of the two-particle vertex. The next step is to include the flow of the two-particle vertex  $\gamma_2^\Lambda$  from the second line in Fig. 1, but still neglect the three-particle vertex  $\gamma_3^\Lambda$  and the frequency dependence of  $\gamma_2^\Lambda$ .<sup>3</sup> Using the vertex flow Eq. (14) with a sharp cutoff and the parametrization (24), we obtain [22]

$$\begin{aligned} \frac{\partial}{\partial \Lambda} U^\Lambda &= \frac{(U^\Lambda)^2}{2\pi} \sum_{\varepsilon=\pm\Lambda} \left[ \tilde{G}_\uparrow^\Lambda(i\varepsilon) \tilde{G}_\downarrow^\Lambda(-i\varepsilon) + \tilde{G}_\uparrow^\Lambda(i\varepsilon) \tilde{G}_\downarrow^\Lambda(i\varepsilon) \right] \\ &= \frac{2(U^\Lambda)^2 V_\uparrow^\Lambda V_\downarrow^\Lambda / \pi}{\left[ (\Lambda + \Gamma)^2 + (V_\uparrow^\Lambda)^2 \right] \left[ (\Lambda + \Gamma)^2 + (V_\downarrow^\Lambda)^2 \right]}, \end{aligned} \quad (30)$$

again with initial condition  $U^{\Lambda=\infty} = U$ .

A systematic improvement with respect to the previous results can be observed in Fig. 4, with the dotted line resulting from the inclusion of the interaction renormalization. The quantitative agreement with the exact results is excellent and holds for  $U/\Gamma = 25$ , the largest value with available Bethe ansatz data [6]. Also for more complex dot geometries this extension considerably improves the agreement with NRG results [22]. We note that a truncated fRG scheme including the full frequency dependence of the two-particle vertex, and hence a frequency dependent self-energy, reproduces also the Kondo resonance and Hubbard bands in the spectral function [20]. This requires, however, a substantial computational effort.

### 3.4 Effect of magnetic fields

We next consider the case of finite magnetic fields. For  $h > 0$  the Kondo resonance in the NRG solution of the spectral function splits into two peaks with a dip at  $\omega = 0$ , resulting in a dip of  $G(V_g)$  at  $V_g = 0$ . In Figs. 5 and 6 we compare the total  $G = G_\uparrow + G_\downarrow$  and partial  $G_\uparrow$  conductance obtained from the above fRG truncation scheme including the flow of the effective interaction with NRG [23] results for different  $h$  expressed in units of  $T_K^{\text{NRG}} = 0.116\Gamma$ , where  $T_K^{\text{NRG}}$  is the width of the Kondo resonance at the particle-hole symmetric point  $V_g = 0$  obtained by NRG [23].

The excellent agreement between NRG and fRG results provides strong evidence of the presence of the Kondo scale within the truncated fRG scheme.

### 3.5 Determining the Kondo scale

From the above comparison of fRG and NRG data shown in Fig. 6 for different  $h$  we infer the appearance of an exponentially small energy scale defining the Kondo

---

<sup>3</sup> Including the frequency dependence of  $\gamma_2^\Lambda$  is an ambitious project that is beyond the scope of this introductory article [20].

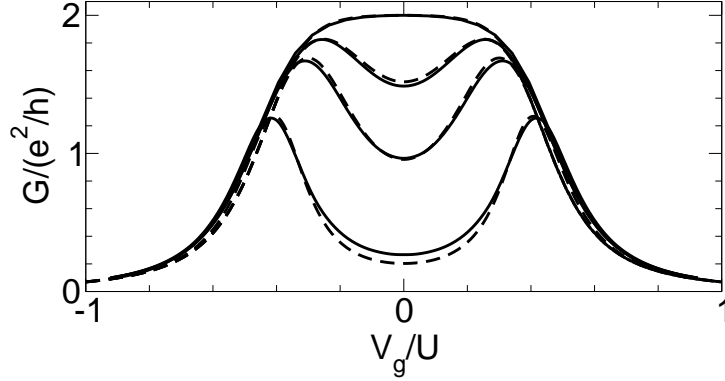


**Fig. 5** Gate voltage dependence of the total conductance  $G$  of a single dot with  $U/\Gamma = 3\pi$  and  $h/\Gamma = 0, 0.058, 0.116, 0.58$  from top to bottom. In units of the  $V_g = 0$  Kondo temperature  $T_K^{\text{NRG}}/\Gamma = 0.116$  these fields correspond to  $h = 0, 0.5T_K^{\text{NRG}}, T_K^{\text{NRG}},$  and  $5T_K^{\text{NRG}}$ . Solid line: NRG data from [23]. Dashed lines: fRG approximation with flow of vertex.

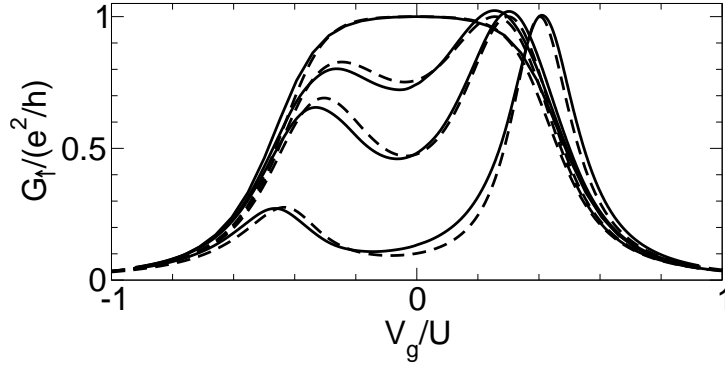


**Fig. 6** Gate voltage dependence of the partial conductance  $G_\uparrow$  of a single dot for the same parameters as in Fig. 5.

scale  $T_K(U, V_g)$  by the magnetic field required to suppress the total conductance to one half of the unitary limit,  $G(U, V_g, h = T_K) = e^2/h$ . For fixed  $U \gg \Gamma$  this definition applies for gate voltages within the resonance plateau for  $h = 0$ . In Fig. 7 we show  $T_K(U, V_g)$  for different  $V_g$  as a function of  $U$  on a linear-log scale. The curves can be fitted to a function of the form

$$f(U/\Gamma) = a \exp \left[ - \left| b \frac{U}{\Gamma} - c \frac{\Gamma}{U} \right| \right] \quad (31)$$

with  $V_g$ -dependent coefficients  $a$ ,  $b$ , and  $c$ . The above form is consistent with the exact Kondo temperature  $T_K$  [1] that depends exponentially on a combination of  $U$  and the level position

$$\begin{aligned}
T_K^{\text{exact}} &\sim \exp \left[ -\frac{\pi}{2U\Gamma} |U^2/4 - V_g^2| \right] \\
&= \exp \left[ -\left| \frac{\pi U}{8\Gamma} - \frac{\pi V_g^2 \Gamma}{2\Gamma^2 U} \right| \right].
\end{aligned} \tag{32}$$

The prefactor of the exponential depends on the details of the model considered. To leading order its  $U$  and  $V_g$  dependence can be neglected. For the fit to Eq. (31) we find  $b(V_g) \approx 0.32$  for all  $V_g$  (see Eq. (29) for comparison), in good agreement with the exact value  $\pi/8 \approx 0.39$ . The prefactor  $a$  depends only weakly on  $V_g$ , and  $c(V_g)$  increases approximately quadratically with  $V_g/\Gamma$  as shown in the inset of Fig. 7, according to the behavior of the exact Kondo temperature Eq. (32). We thus conclude that  $T_K(U, V_g)$  can be determined from the  $h$  dependence of the conductance obtained from the fRG. Similar results are obtained from the local spin susceptibility [1].

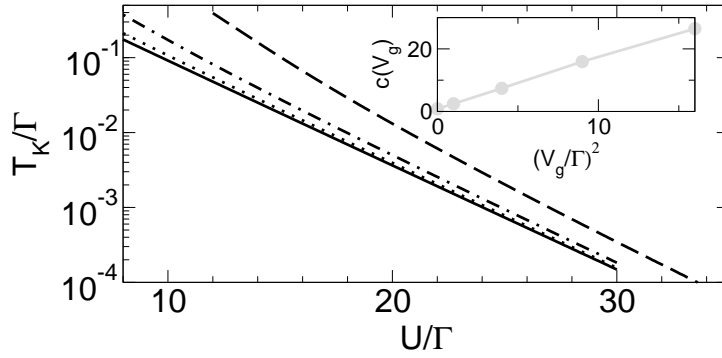


**Fig. 7** The Kondo scale  $T_K$  as a function of  $U$  for different  $V_g$ :  $V_g = 0$  (solid),  $V_g/\Gamma = 1$  (short dashed),  $V_g/\Gamma = 2$  (dotted), and  $V_g/\Gamma = 4$  (long dashed). *Inset*: The fitting parameter  $c$  as a function of  $(V_g/\Gamma)^2$ .

For the single dot at  $T = 0$  the exact conductance, transmission phase, and dot occupancies are directly related by a generalized Friedel sum rule [1]:  $G_\sigma/(e^2/h) = \sin^2(\pi \langle n_\sigma \rangle)$ , and the transmission phase  $\alpha_\sigma = \pi \langle n_\sigma \rangle$ . As  $0 \leq \langle n_\sigma \rangle \leq 1$  the argument of  $\sin^2$  is restricted to a single period and the relation between  $G_\sigma$ ,  $\langle n_\sigma \rangle$ , and  $\alpha_\sigma$  is unique. In many approximation schemes the Friedel sum rule does not hold exactly. In contrast, within our method we map the many-body problem onto an effective single-particle one for which the Friedel sum rule is fulfilled. For gate voltages within the  $h = 0$  conductance plateau the (spin independent) dot filling is  $1/2$  and the (spin independent) phase is  $\pi/2$ . For sufficiently large  $U/\Gamma$  the crossover to  $\langle n_\sigma \rangle = 1$  and  $\alpha_\sigma = \pi$  to the left of the plateau as well as  $\langle n_\sigma \rangle = 0$  and  $\alpha_\sigma = 0$  to the right is fairly sharp.

## 4 Summary and Conclusion

We presented an fRG scheme developed for the study of electronic transport through quantum-dot systems. The resulting differential flow equations describe the effective renormalized level position and interaction in presence of local Coulomb interactions and magnetic fields. Analytical estimates capture signatures of the Kondo effect, and a comparison with exact Bethe ansatz and high-precision NRG results shows excellent agreement up to the largest Coulomb interaction for which Bethe ansatz or NRG data are available.

The presented fRG scheme constitutes a reliable and promising tool in the investigation of correlation effects and interference phenomena in quantum-dot systems. The application to a single quantum dot can be directly extended to different geometries involving more complicated setups [22] such as parallel double dots [24]. In [25] this method was used to investigate the long-standing phase lapse puzzle of the transmission phase through multi-level quantum dots.

Furthermore, the truncated fRG scheme was successfully used to study one-dimensional fermionic lattice models with two-particle interaction and impurities [26, 27, 28, 29] (inhomogeneous Luttinger liquids). In addition to the universal low-energy asymptotics the fRG captures nonuniversal properties at higher energy scales. Novel low-energy fixed points were found for Y-junctions of one-dimensional quantum wires pierced by a magnetic flux [30]. Also a single dot with Luttinger liquid leads [31] was investigated. For the latter the competition between Kondo and Luttinger liquid physics leads to a broad resonance plateau for all experimentally accessible length scales, whereas the low-energy fixed point is described by a sharp resonance characteristic for the Luttinger liquid behavior.

**Acknowledgements** We thank X. Barnabé-Thériault, R. Hedden, W. Metzner, Th. Pruschke, H. Schoeller, U. Schollwöck, and K. Schönhammer for useful discussions. We thank T. Costi and J. von Delft for providing their NRG and Bethe ansatz data. This work has been supported by the French ANR (program PNANO) (S.A.), the Deutsche Forschungsgemeinschaft (SFB 602) (V.M.), and a Feoder Lynen fellowship of the Alexander von Humboldt foundation and the Istituto Nazionale di Fisica della Materia–SMC–CNR (T.E.).

## References

1. A.C. Hewson, *The Kondo Problem to Heavy Fermions* (Cambridge University Press, Cambridge, UK, 1993)
2. A.M. Tsvelik, P.B. Wiegmann, *Adv. Phys.* **32**, 453 (1983)
3. L. Glazman, M. Raikh, *JETP Lett.* **47**, 452 (1988)
4. T.K. Ng, P.A. Lee, *Phys. Rev. Lett.* **61**, 1768 (1988)
5. T.A. Costi, A.C. Hewson, V. Zlatić, *J. Phys.: Condens. Matter* **6**, 2519 (1994)
6. U. Gerland, J. von Delft, T.A. Costi, Y. Oreg, *Phys. Rev. Lett.* **84**, 3710 (2000)
7. Y. Meir, N.S. Wingreen, *Phys. Rev. Lett.* **68**, 2512 (1992)
8. D. Goldhaber-Gordon, H. Shtrikman, D. Mahalu, D. Abusch-Magder, U. Meirav, M.A. Kastner, *Nature* **391**, 156 (1998)

9. W.G. van der Wiel, S.D. Franceschi, T. Fujisawa, J.M. Elzerman, S. Tarucha, L.P. Kouwenhoven, *Science* **289**, 2105 (2000)
10. K.G. Wilson, *Rev. Mod. Phys.* **47**, 773 (1975)
11. H.R. Krishna-murthy, J.W. Wilkins, K.G. Wilson, *Phys. Rev. B* **21**, 1044 (1980)
12. W. Hofstetter, J. König, H. Schoeller, *Phys. Rev. Lett.* **87**, 156803 (2001)
13. M. Salmhofer, C. Honerkamp, *Prog. Theor. Phys.* **105**, 1 (2001)
14. J.W. Negele, H. Orland, *Quantum Many-Particle Systems* (Addison-Wesley, Reading, 1987)
15. T. Enss, Renormalization, conservation laws and transport in correlated electron systems, Ph.D. thesis, University of Stuttgart, Germany (2005), [arXiv:cond-mat/0504703](https://arxiv.org/abs/cond-mat/0504703), URL <http://elib.uni-stuttgart.de/opus/volltexte/2005/2258/>
16. W. Metzner, *AIP Conf. Proc.* **846**, 130 (2006)
17. F.J. Wegner, A. Houghton, *Phys. Rev. A* **8**, 401 (1973)
18. J. Polchinski, *Nucl. Phys. B* **231**, 269 (1984)
19. C. Wetterich, *Phys. Lett. B* **301**, 90 (1993)
20. R. Hedden, V. Meden, Th. Pruschke, K. Schönhammer, *J. Phys.: Condens. Matter* **16**, 5279 (2004)
21. T.R. Morris, *Int. J. Mod. Phys. A* **9**, 2411 (1994)
22. C. Karrasch, T. Enss, V. Meden, *Phys. Rev. B* **73**, 235337 (2006)
23. T.A. Costi, *Phys. Rev. B* **64**, 241310(R) (2001)
24. V. Meden, F. Marquardt, *Phys. Rev. Lett.* **96**, 146801 (2006)
25. C. Karrasch, T. Hecht, Y. Oreg, J. von Delft, V. Meden, *Phys. Rev. Lett.* **98**, 186802 (2007)
26. V. Meden, W. Metzner, U. Schollwöck, K. Schönhammer, *Phys. Rev. B* **65**, 045318 (2002)
27. S. Andergassen, T. Enss, V. Meden, W. Metzner, U. Schollwöck, K. Schönhammer, *Phys. Rev. B* **70**, 075102 (2004)
28. T. Enss, V. Meden, S. Andergassen, X. Barnabé-Thériault, W. Metzner, K. Schönhammer, *Phys. Rev. B* **71**, 155401 (2005)
29. S. Andergassen, T. Enss, V. Meden, W. Metzner, U. Schollwöck, K. Schönhammer, *Phys. Rev. B* **73**, 045125 (2006)
30. X. Barnabé-Thériault, A. Sedeki, V. Meden, K. Schönhammer, *Phys. Rev. Lett.* **94**, 136405 (2005)
31. S. Andergassen, T. Enss, V. Meden, *Phys. Rev. B* **73**, 153308 (2006)